Experimental Investigation of Electron Collection to Solid and Slotted Tape Probes in a High-Speed Flowing Plasma

Éric Choinière, *Member, IEEE*, Sven G. Bilén, *Member, IEEE*, Brian E. Gilchrist, *Senior Member, IEEE*, Keith R. Fuhrhop, *Student Member, IEEE*, and Alec D. Gallimore

***Abstract*—This paper presents the analysis and comparison of measurements of electron current collection to round cylinder, solid tape, and slotted tape electrodynamic-tether samples in a mesosonic flowing plasma. A Hall thruster was used to simulate a flowing unmagnetized space plasma in a large 6-m × 9-m vacuum chamber. Guarded tether samples were employed to mitigate end effects. Plasma parameters were determined based on the ion saturation and electron retardation regimes of a cylindrical Langmuir probe's current characteristics. Solid tape samples with widths spanning from 4.9 to 41.9 Debye lengths, and slotted tapes with center-to-center line spacings spanning from 1.4 to 13.2 Debye lengths were tested. Several conclusions can be drawn from the analysis of the results: 1) the plasma flow leads to significant current enhancements over that predicted by the orbital-motion-limited theory; 2) the electron current collected per unit area on solid tapes decreases as the width of the tape is increased; 3) beyond a threshold bias close to the beam energy, solid and slotted tapes both collect more current when oriented transverse to the flow; 4) slotted tapes are more efficient electron collectors per unit area than solid tapes; and 5) our data suggests that the electron current collected on slotted tapes decreases with increasing line spacing until a possible minimum is attained, beyond which it is expected to start increasing again. The minimum was attained in the case of the samples oriented transverse to the flow, but not in the case of the samples aligned with the flow, for which the critical spacing is likely higher (due to an increased sheath interaction radius of each line caused by flow-induced sheath elongation).**

***Index Terms*—Bare electrodynamic tethers, high-voltage sheath, Langmuir probes, orbital-motion-limited sheath, plasma current collection, plasma flow.**

Manuscript received April 6, 2004; revised April 29, 2005. This work was supported in part by NASA under Contract NAS8-99 128. The work of É. Choinière was supported in part by the University of Michigan's Horace H. Rackham School of Graduate Studies, in part by the Natural Sciences and Engineering Research Council of Canada, and in part by the Communications Research Centre (Canada).

É. Choinière is with the Radiation Laboratory, Department of Electrical Engineering and Computer Science, University of Michigan, Ann Arbor, MI 48109 USA, and also with Defence Research and Development Canada, Ottawa, ON, K1A 0Z4 Canada (e-mail: echoinie@umich.edu).

S. G. Bilén is with the Communications and Space Sciences Laboratory, Department of Electrical Engineering, The Pennsylvania State University, University Park, PA 16802 USA (e-mail: sbilen@psu.edu).

B. E. Gilchrist is with the Radiation Laboratory, Department of Electrical Engineering and Computer Science, and the Space Physics Research Laboratory, Department of Atmospheric, Oceanic and Space Sciences, University of Michigan, Ann Arbor, MI 48109 USA (e-mail: gilchrst@umich.edu).

K. R. Fuhrhop is with the Radiation Laboratory, Department of Electrical Engineering and Computer Science, University of Michigan, Ann Arbor, MI 48109 USA (e-mail: kfuhrhop@umich.edu).

A. D. Gallimore is with the Plasmadynamics and Electric Propulsion Laboratory, Department of Aerospace Engineering, University of Michigan, Ann Arbor, MI 48109 USA (e-mail: alec.gallimore@umich.edu).

Digital Object Identifier 10.1109/TPS.2005.852366

I. Background

THE USE of a bare section of a space-borne electrodynamic tether as an electron-collection device has been suggested [1] to be a promising alternative to end-body electron collectors for certain applications, provided that electrons are collected in a quasi-orbital-motion-limited regime. For a given bias potential, plasma probe theory predicts that the collected electron current per unit area is maximized in the orbital-motion-limited regime, which is only valid with sufficiently thin wires [2].

The bare tether concept was to be first tested during NASA's Propulsive Small Expendable Deployer System (ProSEDS) mission [3]. Although now canceled [4], the concept is being considered for future missions. Present bare tether designs, such as the one designed for the ProSEDS mission, use a small, closely packed cross-section of wires or even a single wire as the anode. In future designs, addressing concerns such as survivability to collisions with micro-meteoroids and space debris will require the use of distributed or sparse tether cross-section geometries, which could span tens of Debye lengths depending on plasma density and temperature [5].

Since collected current per unit area is maximized in the orbital-motion-limited regime of single thin cylinders, one needs to consider how these new distributed or sparse geometries will perform in terms of electron current collection, as compared to thin cylinders. In addition, the effect of the high-speed flow on the electron collection to these alternative geometries, as well as to thin cylinders, has yet to be clearly understood. Ultimately, designers will need to know how to configure a tether for adequate survivability and minimum mass, for example.

In this paper, the orbital-motion limit (OML) will be used as a baseline when comparing the current collection results for various sample geometries and sizes. Recall that the OML electron current collected by a thin cylinder is given by [2], [6]

$$I = \underbrace{A_p n_e e \sqrt{\frac{eT_e}{2\pi m_e}}}_{I_{\rm the}} \left\{ \frac{2}{\sqrt{\pi}} \sqrt{\frac{V_0 - V_p}{T_e}} + \exp\left(\frac{V_0 - V_p}{T_e}\right) \operatorname{erfc}\left(\sqrt{\frac{V_0 - V_p}{T_e}}\right) \right\} \quad (1)$$

with $\operatorname{erfc}(x) = (2/\sqrt{\pi}) \int_x^\infty e^{-t^2} dt$. Equation (1) is approximated, for $V_0 - V_p > 2T_e$, by

$$I = \underbrace{A_p n_e e \sqrt{\frac{eT_e}{2\pi m_e}}}_{I_{\rm the}} \frac{2}{\sqrt{\pi}} \sqrt{1 + \frac{V_0 - V_p}{T_e}} \quad (2)$$

TABLE I
DRAWING AND DESCRIPTION OF THE SIX GUARDED TETHER SAMPLES SHOWN BEFORE ASSEMBLY. THE LENGTHS INDICATED IN THE DRAWING ARE IN mm (30-mm PROBE, 60-mm GUARDS)

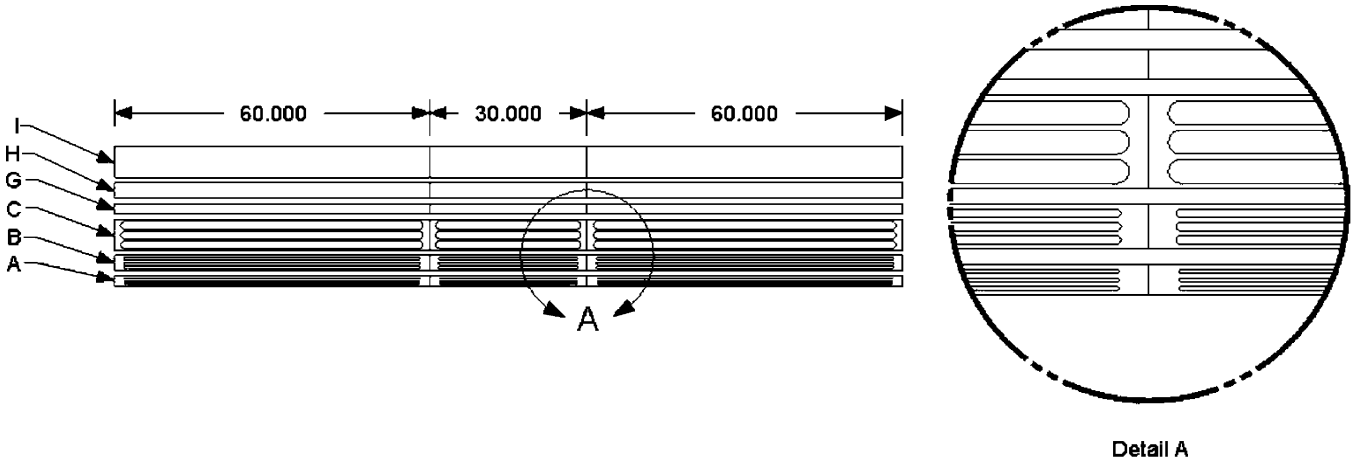

Sample	Description	Width (mm)	Feature Description
A	4 lines, 3 slots, 28% porosity	1.95	Slot width: 0.20 mm, line width: 0.34 mm
B	4 lines, 3 slots, 50% porosity	2.89	Slot width: 0.51 mm, line width: 0.34 mm
C	4 lines, 3 slots, 75% porosity	5.95	Slot width: 1.53 mm, line width: 0.34 mm
G	Narrow Solid Tape	1.95	N/A
H	Medium Solid Tape	2.89	N/A
I	Wide Solid Tape	5.95	N/A

where V_0 is the bias voltage, V_p is the plasma potential, T_e is the electron temperature in eV, A_p is the cylinder area, and $I_{\rm the}$ is the electron thermal current.[1] The latter is given as a function of the electron number density n_e (in m^{-3}), the electron mass m_e, and the electron charge magnitude e. In an effort to facilitate comparisons of current characteristics for various geometries with OML theory, and in order to provide a minimal-parameter dataset for future reference, our results are presented in a normalized format, showing the normalized current $I_n = I/I_{\rm the}$ as a function of the normalized bias voltage $\phi_0 = (V_0 - V_p)/T_e$, which in the case of OML yields the simplified equation

$$I_n = \frac{2}{\sqrt{\pi}}\sqrt{\phi_0} + \exp(\phi_0)\mathrm{erfc}(\sqrt{\phi_0}) \approx \frac{2}{\sqrt{\pi}}\sqrt{1+\phi_0}. \quad (3)$$

For large voltages, (3) is independent of the temperature T_e, since both the right-hand side and left-hand side are then proportional to $1/\sqrt{T_e}$. This normalization allows one to directly compare our experimental results, which involve various tether geometries in a flowing plasma, against OML theory.

Previous experimental data [7] indicated that a tape width of 6.9 Debye lengths would collect about 85%–90% of the electron current collected by an equal-area round cylinder, and that the perpendicular tape orientation, with respect to plasma flow, would consistently outperform the parallel orientation in terms of collected current.

In this paper, we describe the results of a new set of chamber tests that were intended to address questions of end effects and plasma source current limitations discussed by Gilchrist *et al.* [7], in addition to testing a larger range of "solid tape" widths and a new "slotted tape" geometry with various porosities. The issue of end effects was addressed by adding guards to the tether samples, which are described below. The question of possible plasma source current limitations, raised by Gilchrist *et al.* [7], was resolved by modifying the plasma source parameters, as discussed in Section III.

[1]All units used in this work are MKS except for temperature, which is specified in electronvolts (eV).

II. DESIGN AND ASSEMBLY OF SOLID AND SLOTTED TAPE TETHER GUARDED SAMPLES

The tether samples tested here, in addition to a thin cylindrical reference sample, included solid tape samples in three different widths, and slotted tape samples of corresponding widths having three different porosity levels. The details of these designs, as well as a drawing of the samples and their characteristic sizes, are given in Table I. Each of the six solid and slotted tapes were tested in two different orientations (parallel and perpendicular to the plasma flow) and, along with the reference sample, at three different distances from our plasma source. Tungsten metal was used for all samples to ensure that they would endure the expected high temperatures that are caused by the collection of high-energy electrons at the samples' surfaces. Nonetheless, a low duty cycle pulsing of the applied voltages was necessary to allow the samples to cool off, thus preventing melting; details of this procedure were reported by Gilchrist *et al.* [7].

The diameter of the reference cylinder and widths of the three solid tape samples are given in Table II in terms of the Langmuir-probe-determined local Debye length at the three chamber test positions. The reference cylinder's diameter, spanning from 0.7 to 2.0 Debye lengths depending on position, was sufficiently thin to collect electron current under conditions close to that of the OML regime in a stationary plasma. The solid tape widths spanned from 4.9 to 41.9 Debye lengths, extending the range of previously tested widths, which spanned from 6 to 19 Debye lengths [7].

TABLE II
DIAMETER OF THE REFERENCE CYLINDER AND WIDTHS OF THE THREE SOLID TAPES AT ALL THREE LOCATIONS, EXPRESSED IN TERMS OF THE LOCAL DEBYE LENGTH

Pos.	Ref. Cyl.	Solid Tape		
		Narrow	Medium	Wide
75 cm	2.0	13.7	20.4	41.9
160 cm	1.1	7.4	11.0	22.6
300 cm	0.7	4.9	7.2	14.9

TABLE III
CENTER-TO-CENTER LINE SPACING AS A FUNCTION OF SAMPLE POROSITY AT ALL THREE LOCATIONS, EXPRESSED IN TERMS OF THE LOCAL DEBYE LENGTH

Position	Slotted Tapes by Porosity		
	28%	50%	75%
75 cm	3.8	6.0	13.2
160 cm	2.1	3.2	7.1
300 cm	1.4	2.1	4.7

The three slotted samples were designed with the same overall widths as their solid counterparts; this strategy allows us to directly compare solid and porous samples spanning equivalent widths. In addition, the design is such that each of the four lines on every slotted sample has the same perimeter as the reference cylinder, allowing one to consider the effects and measure the extent of sheath interactions. The center-to-center spacings of the slotted samples are given in Table III in terms of the Debye length.

Since our primary interest is very long electrodynamic tethers, a technique was sought to mitigate any probe end effects. For this purpose, guards were included in all of our tether sample assemblies. Each guard is essentially identical to the center section and is biased at the same potential. The guards, which are each 6 cm in length while the center probe itself is 3 cm long, are shown in Table I and Fig. 1, together with the probes. The effect of the guards is to extend the cylindrical sheath to the full length of the sample, that is, five times the length of the center probe on which current is measured.

Schematics of the full assemblies of the guarded tether samples are shown in Fig. 1. Due to the very small thickness of the tungsten samples under consideration here (0.1 mm thick), it was not possible to feed the center probe using a wire that would have been inserted in one of the guards, as is typically done on some larger tri-axial Langmuir probes. Instead, the center feed wire runs through an oblique ceramic tube and connects to the center probe at one of its ends. On all samples, the feed wires to both the guards and the probe were soldered to the center conductor of a bulk-head SHV (safe high voltage) connector. The connector-sample interfaces were then covered with vacuum epoxy. The aluminum support structure for the SHV connectors provided a localized ground.

The probe and guards also had to be physically attached but electrically insulated from each other. Ceramic joints were used to this effect, an example of which is shown in Fig. 2, and were attached to the tungsten probes and guards using stainless-steel machine screws that were then carefully sanded down into a flat surface in order to best emulate the surface of the sample. The portion of the surface area of the ceramic joint covering the tungsten probe and not covered by the screw head was accounted for in the calculation of the total area of each probe.

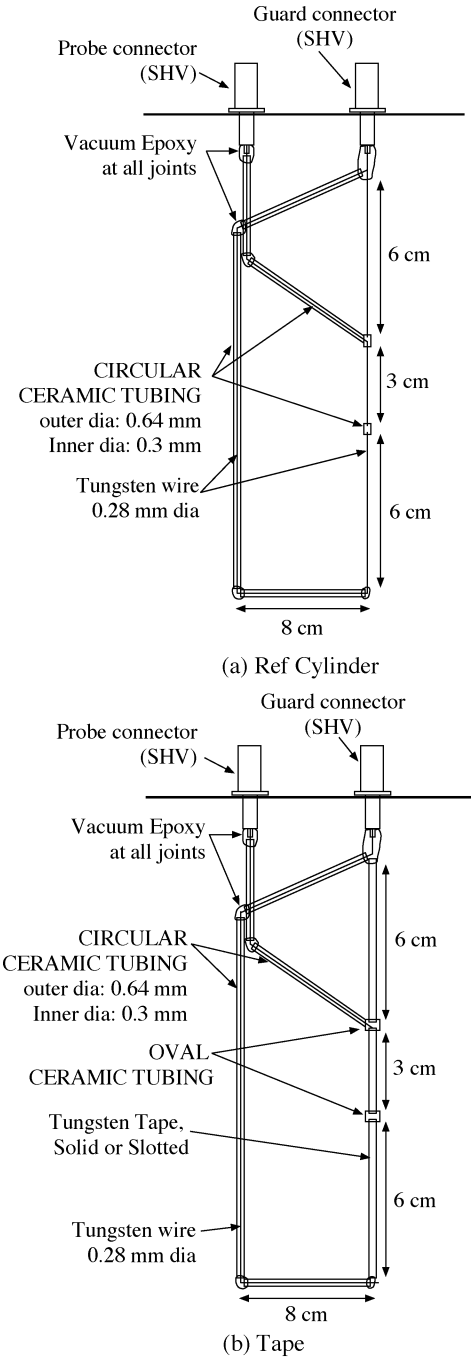

Fig. 1. Assemblies of the (a) reference cylinder and (b) tape guarded tether samples.

Fig. 3 shows pictures of three of our tether sample assemblies: the reference cylinder, the wide solid tape, and the 75%-porous wide slotted tape. The solid and slotted samples are shown with both SHV connectors installed, while the reference cylinder sample is shown prior to the installation of the connectors.

III. VACUUM CHAMBER SETUP AND PLASMA SOURCE CHARACTERISTICS

Our vacuum chamber tests were performed using the Large Vacuum Test Facility (LVTF), a 9-m by 6-m cylindrical stainless-steel-clad tank located within the Plasmadynamics and Electric Propulsion Laboratory (PEPL) at the University of

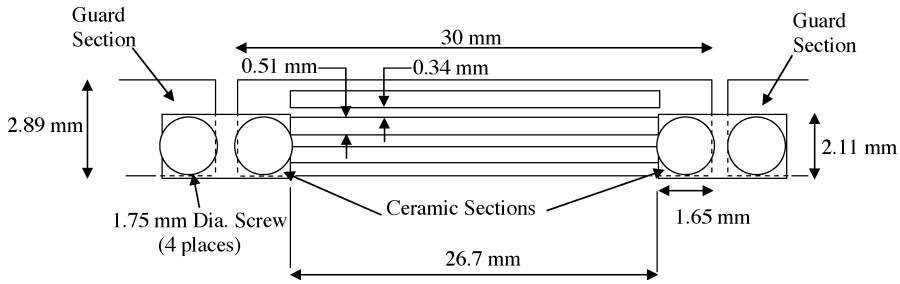

Fig. 2. Example of the ceramic attachment used on all solid and slotted tape samples to attach the probe and guards while preserving electrical isolation. Dimensions shown here correspond to the medium slotted probe (sample B in Table I).

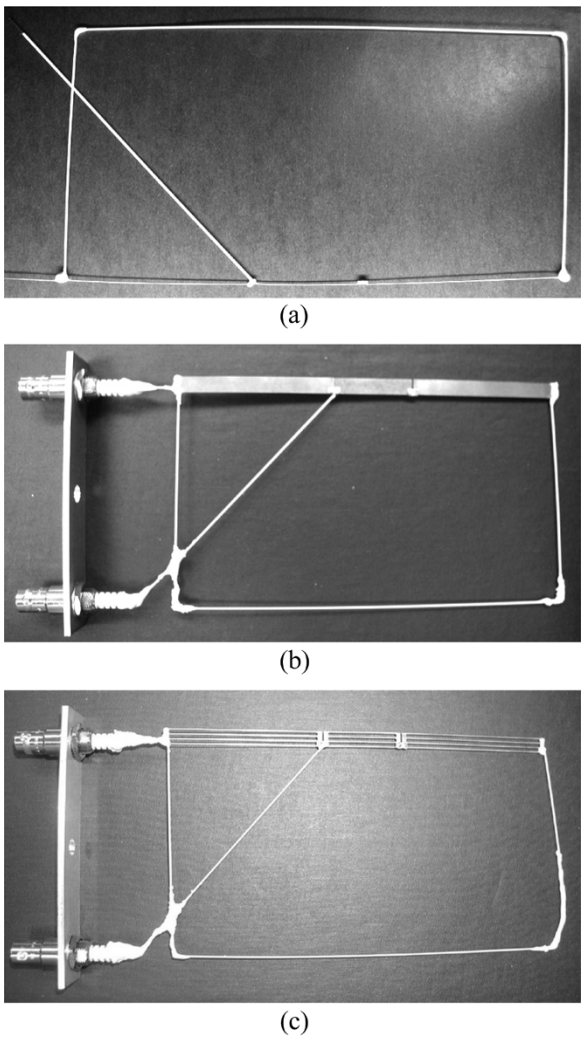

Fig. 3. Pictures of three typical tether samples. (a) 0.28-mm diameter reference cylinder. (b) 5.95-mm-wide solid tape. (c) 75%-porous wide slotted tape.

Michigan, Ann Arbor. For this experiment, four of the seven available nude cryopumps were used to reach a high vacuum.

Fig. 4 shows a diagram of the experimental setup within the LVTF. Two positioning tables were used to change the separation distance between the thruster and sample plane and to locate the sample under test directly along the thruster's centerline. The thruster was mounted on a table (the $x-y$ table) that could move axially over a 1.0-m range and over a sufficient radial range to cover all samples. The samples were mounted on an aluminum frame that was connected to the other table

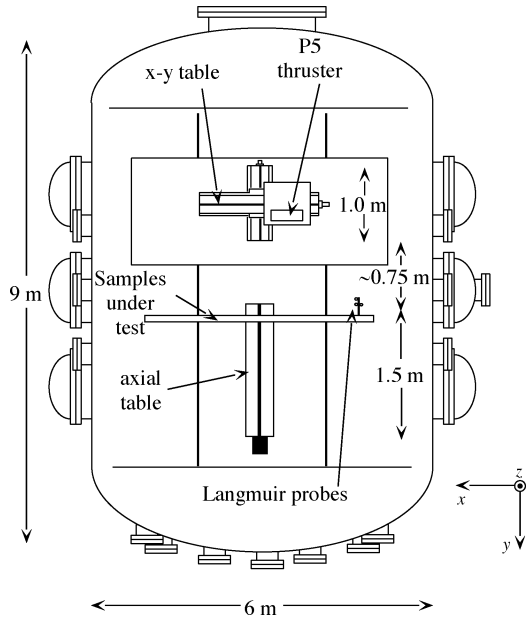

Fig. 4. Experimental setup in the LVTF at the PEPL.

(the *axial* table) that could span a 1.5-m axial range. Combined table movement allowed thruster–sample separation distance to change from 0.75 to 3 m; our tests were performed at 0.75 m, 1.60 m, and 3.00 m from the thruster. Changing separation distance was the primary mechanism for changing the plasma density seen at the sample plane.

Fig. 5 shows an overall picture of the aluminum structure supporting our tether samples and Langmuir probes, together with the Hall thruster used as a plasma source. The latter is a 5 kW-class Hall thruster named "P5," which was developed by the PEPL and the Air Force Research Laboratory; more detail is given by Haas *et al.* [8]. For these tests, the thruster was set at off-nominal conditions in order to lower the plasma velocity and density seen along the thruster's axial direction. Its operating conditions are given in Table IV. The primary changes in those settings from the ones used in the two data sets presented by Gilchrist *et al.* [7] are the discharge current, which was raised from 4–5.3 A to 12.5 A, and the anode flow rate, which had to be raised from 45–60 sccm to 112.1 sccm to support the increased discharge current.

Assessment of the emitted beam energy was performed using two different techniques. Laser-induced fluorescence (LIF) measurements using the off-axis multiplex technique have provided an estimate of 43 eV [9], whereas Langmuir probe

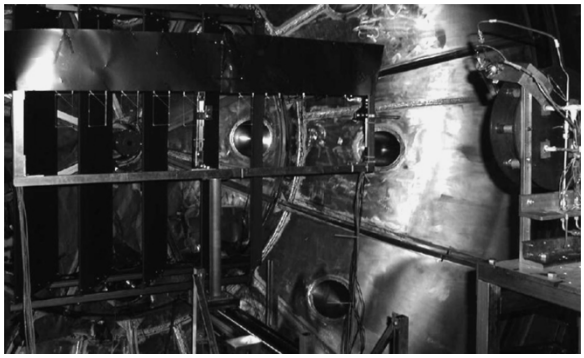

Fig. 5. (left) Picture of the guarded sample support structure and (right) P5 Hall thruster used as a high-speed plasma source.

TABLE IV
OPERATING PARAMETERS OF THE PLASMA SOURCE (P5 HALL THRUSTER)

Maximum Chamber Pressure	9.1 μtorr
Discharge Voltage, V_d	100 V
Discharge Current, I_d	12.5 A
Inner Magnet Current, I_{im}	3.0 A
Outer Magnet Current, I_{om}	2.0 A
Cathode Voltage, V_c	$[-17, -18]$ V
Heater Voltage, V_{htr}	8.3 V
Anode Flow rate, $\dot{m}_a$	112.1 sccm
Cathode Flow rate, $\dot{m}_c$	6.0 sccm

(LP) measurements in the ion saturation regime (discussed in the Appendix) have yielded a value of 25 eV. More detail regarding the off-axis multiplex LIF measurement technique is given by Gilchrist *et al.* [7] and Williams *et al.* [10]. It should be noted that the LP value of 25 eV is close to, if not within, the bounds of the error in the LIF-determined beam energy value, which is about 38%, given that the relative error in the velocity determined using the multiplex technique was about 19%. This relative error[2] is obtained from the ratio of the absolute error in velocity, which was about 1.5 km/s [11], to the value of the measured velocity, 7.95 km/s. Here we note that this particularly large relative error is due to the operation of the P5 Hall thruster at off-nominal conditions, with an unusually low discharge voltage. At higher beam velocities, the absolute error of 1.5 km/s results in a much lower relative error. Also, recent improvements of the LIF measurement technique, using an "axial injection" procedure [11], have allowed significant improvements in the accuracy of the beam velocity measurements and will be used in future experiments.

The values given for both the LIF and LP measurements were measured 75 cm away from the thruster on its centerline axis. According to the LIF measurement, the ions have an offset Maxwellian distribution, with a directed energy as given above, and a temperature of about 0.4 eV at 75 cm. The electron temperature, as determined by the LP measurements, varied as a function of position between 1.47 eV and 1.80 eV (see Table V).

A schematic of the current–voltage measurement system is given in Fig. 6. We connected a Universal Voltronics BRC 20 000 high voltage (HV) power supply to the tether samples through a high-voltage relay box inside the chamber. The HV power supply was controlled via RS-232 by the computer controller running a custom virtual instrument (VI) under LabVIEW. The computer commanded the HV power supply to a specified voltage and then quickly back to zero (within 50 to 100 ms), followed by several seconds of cool-down to minimize sample heating. Current measurement on the sample probes was achieved using an American Aerospace Controls 835-2-10 current sensor; increased current sensitivity was obtained by looping the HV supply line ten times through the sensor. The current to the sample guards was measured separately using a F.W. Bell ma-2000 current sensor. An HP 34970 data acquisition unit was used to measure the voltage signals generated by both current sensors. The data were recorded as triplets containing the applied voltage, the probe current, and the guard current.

[2]Note: $(m_i(7950\ \text{m/s})^2/2e) \approx 43$ eV with $m_i = 2.18 \times 10^{-25}$ kg for Xe^+.

TABLE V
VARIATION OF THE MEASURED PLASMA PARAMETERS AS A FUNCTION OF DISTANCE FROM THE HALL THRUSTER. MEASUREMENTS WERE PERFORMED USING THE ION SATURATION AND ELECTRON RETARDATION DATA FROM A TRANSVERSE LP. THE BEAM ENERGY VALUE DETERMINED USING THE LP IS 25 eV. THE "BEAM FRACTION", μ_b, INDICATES THE FRACTION OF ALL IONS THAT ARE BELIEVED TO BE BEAM (HIGH-SPEED) IONS. DENSITY, TEMPERATURE AND DEBYE LENGTH ESTIMATES HAVE ABOUT 8%, 5% AND 6.5% ACCURACY, AS DISCUSSED IN THE APPENDIX

Position	n_e (m^{-3})	T_e (eV)	λ_{De} (mm)	μ_b
75 cm	4.95×10^{15}	1.80	0.14	95%
160 cm	1.37×10^{15}	1.72	0.26	53%
300 cm	0.51×10^{15}	1.47	0.40	32%

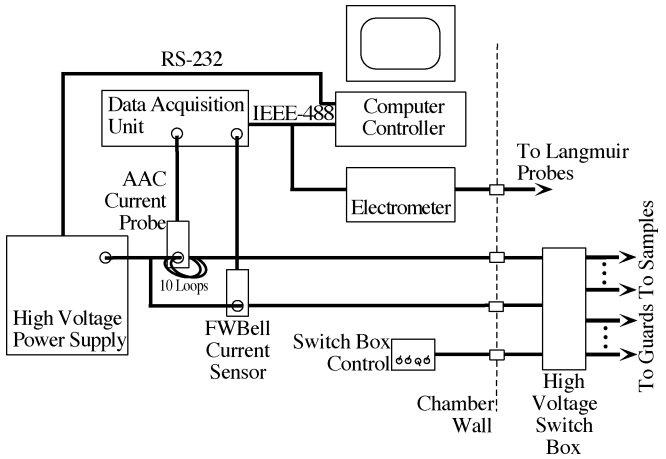

Fig. 6. Schematic of the computer-controlled high-voltage test equipment setup.

IV. PLASMA PARAMETER MEASUREMENTS USING NEGATIVELY-BIASED LANGMUIR PROBES

Plasma density, temperature, flow speed, and the fraction of beam ions to background ions were determined using a 4-cm long, vertically oriented (i.e., perpendicular to the flow) LP with a diameter of 0.28 mm (same diameter as our reference cylinder sample). All LP sweeps were performed using a Keithley 2410 source electrometer controlled via a custom LabVIEW script running on a personal computer.

The plasma parameters, shown in Table V, were extracted from the ion saturation (OML regime) and electron retardation regions of the *I–V* characteristics using a LP oriented transverse to the direction of the flow. In the OML regime, there are several advantages to selecting the ion saturation as opposed to the electron saturation region for parameter extraction. An ion-attracting cylindrical probe oriented transverse to the flow in a high-speed plasma is known to be virtually free of end effects [12]. In addition, a simple but fairly accurate ion collection model is available that accounts for the velocity of the flow in the ion saturation regime [13]. By contrast, there are currently no accurate models for the electron collection to an electron-attracting probe that can account for the plasma flow. In the mesosonic regime, where the plasma flow is much faster than the thermal ion velocity yet much slower than the electron thermal velocity, important sheath asymmetries and elongations exist in the electron-attracting mode that get stronger with the applied bias, which makes the prediction of collected current a complex problem. One of the aims of the experimental work presented here is, in fact, to improve the understanding of the macroscopic effect of plasma flow on electron collection. An accurate model of electron collection in flowing plasmas is also currently being developed [14]–[16]. Finally, using a negatively-biased LP provides an independent assessment of the plasma parameters, since all our test samples were biased positively.

The procedure that was used for the plasma parameter extraction from the LP current characteristics is detailed in the Appendix. In addition to providing plasma density and temperature readings, our analysis quantifies the ion "beam fraction" and describes what appears to be effective workfunction variations.

The results of this analysis indicate the existence of a population of thermal ions far from the high-speed plasma source, which is born out of cumulative charge-exchange collisions between the incident high-speed ions and the neutral background xenon gas. The number-density ratio of high-speed ions to thermal ions is quantified in Table V and ranges from an estimated 95% at the closest distance (75 cm) to 32% at the farthest distance (300 cm). This fall-off of the fraction of beam ions can be fitted to an equivalent "ion beam survival characteristic distance" of 2.14 m, which is just short of the theoretical charge-exchange mean free path of 2.6 m corresponding to the measured background pressure and ion energy, and assuming a background neutral temperature of 350 K. The fall-off is likely due to a combination of effects, such as the beam loss through charge-exchange collisions and the geometrical divergence of the ion beam, combined with a uniform thermal ion population. Geometrical divergence may explain the smaller value measured for the beam survival characteristic distance (2.14 m) as compared to the theoretical prediction (2.6 m).

V. Comparison of Chamber and Ionospheric Environments

Here we describe how the plasma environment created in our vacuum chamber tests compares with the ionospheric plasmas applicable to space tethers, specifically with regard to Debye length and magnetic field effects.

A. Scaling of Tether Samples

As the reader may have noticed in Table V, the laboratory plasma densities were a few orders of magnitude larger than those applicable to electrodynamic tethers in the ionosphere, and the measured temperatures were about one order of magnitude larger. This resulted in Debye lengths one to two orders of magnitude smaller than those found in the ionosphere in low-Earth orbits. Bare tether designs of interest for use in the ionosphere will generally have cross-sectional dimensions on the order of the local Debye length. Therefore, in order to produce meaningful results, the cross sections of our experiment samples were scaled to dimensions on the order of the experimentally measured Debye length and somewhat larger, so that we could experimentally test the limits of applicability of the OML regime.

Additionally, when comparing ionospheric bare tether systems with our chamber tests, the net bias potential $V_0 - V_p$ must be scaled with respect to the electron temperature T_e. The resulting normalized bias $\phi_0 = (V_0 - V_p)/T_e$ is dimensionless, and allows comparisons with real space systems. The range of the normalized bias potential ϕ_0 provided by our data covers from about -10 to $+175$. Although real ionospheric-based tether systems will potentially have normalized bias potentials of up to a few thousand, our data set does provide meaningful results that will improve the understanding of the electron collection to bare tethers even at these higher bias potentials.

B. Geomagnetic Field Effects

Table VI lists the geomagnetic-field parameters applicable to our vacuum chamber tests as well as typical ionospheric conditions relevant to electrodynamic tethers. The geomagnetic flux density was weaker inside our chamber than it is in the ionosphere by about a factor of 4 [17].

In order to qualitatively evaluate the importance of the geomagnetic field effect on electron current collection in our chamber tests and in the ionosphere, it is helpful to compare the electron gyroradius with the expected dimensions of the sheath size surrounding the biased tether. The electron gyroradius is computed via the equation $r_G = (m_e/e)(\overline{v}/B)$, where B is the geomagnetic flux density (in tesla), and $\overline{v}$ is a representative value for the average velocity of an electron.

In the background plasma, the average velocity $\overline{v} = \sqrt{8eT_e/\pi m_e} = \sqrt{(8/\pi)}v_{\rm the}$, where $v_{\rm the}$ is the electron thermal velocity. However, within the sheath, the thermal velocity $v_{\rm the}$ no longer is representative of the velocity of electrons, which will have been accelerated by the sheath's electric field. When the effect of the accelerating sheath is taken into account, the gyroradius within the sheath varies anywhere from the value obtained in the background plasma up to a maximum value corresponding to the maximum velocity that an electron may acquire within the sheath, $v_{\max} = \sqrt{(2e(V_0 - V_p))/m_e}$.

In the vacuum chamber, the background plasma's electron gyroradius ($r_{GB} = 0.52$ m) is much larger than the approximate size of the sheath ($R_s = 0.004$ m) predicted by kinetic simulations [16], which implies that the effects of the geomagnetic field on electron collection is negligible. On the contrary, the ionospheric plasma's electron gyroradius ($r_{GB} = 0.03$ m)

TABLE VI
COMPARISON OF SHEATH DIMENSIONS AND IN-SHEATH ELECTRON GYRORADIUS FOR VACUUM CHAMBER EXPERIMENTS AND TYPICAL IONOSPHERIC CONDITIONS RELEVANT TO ELECTRODYNAMIC TETHERS

Parameters of Interest	Vacuum Chamber	Ionosphere
Geomagnetic Flux Density B (T) [17]	9×10^{-6}	36×10^{-6}
Electron Temperature T_e (eV)	1.5	0.1
Representative Bias Voltage	150 T_e	10000 T_e
Representative Debye length (m)	0.0003	0.008
"Background" Electron Gyroradius r_{GB} (m)	0.52	0.03
Maximum In-Sheath Electron Gyroradius r_{GS} (m)	4.6	2.7
Sheath Size Scale R_s (m) [16]	0.004	1

is quite small compared to the expected sheath size of 1 m, which could lead us to believe that the geomagnetic field could be expected to have significant effects, unlike our chamber test conditions. However, when we consider the *accelerated* in-sheath gyroradius, which may be as large as 2.7 m, then we conclude that an electron would only experience a fraction of a gyration during its transit through the sheath. Therefore, the geomagnetic field is expected to have only a second-order effect on the electron collection process for the typical ionospheric conditions of relevance to electrodynamic tethers. This conclusion supports the applicability of the experimental results presented here for the design of bare electrodynamic-tether systems.

VI. EXPERIMENTAL RESULTS AND ANALYSIS

Our results are presented in four parts: the reference cylinder, the solid tapes, the slotted tapes, and, finally, a comparison of the solid and slotted tapes. All results are presented in the normalized form I_n vs. ϕ_0, where $I_n \equiv (I/I_{\rm the})$ and $\phi_0 \equiv ((V_0 - V_p)/T_e)$. The values used for the temperature T_e and the electron thermal current $I_{\rm the}$ are based on the Langmuir probe-measured electron temperature and plasma density, as detailed in Section IV. The collected current is normalized to the electron thermal current $I_{\rm the}$ collected at the plasma potential, as defined by (1). A theoretical plot of OML current, scaled this way, would result in the expression given by (3) and would be independent of temperature, as discussed in the Introduction. This normalization provides a means of evaluating the performance of various probes by comparing them to OML theory, as well as by comparing their current characteristics in terms of collected current per unit area. Note that the extent of the axis of the normalized voltage ϕ_0 varies from one test position to another, due to differences in the electron temperatures (used in the normalization) measured at the three positions, and from variations in the collected voltage data range.

A. Reference Cylinder

Fig. 7 shows the normalized results for the reference cylinder at the three test distances from the plasma source (along with solid tape data). The reference cylinder at 75 cm is seen to collect much more current than that predicted by OML theory, by as much as 40% at a bias of 100 T_e. This enhancement is seen to decrease as we move away from the thruster to 160 cm and 300 cm. In fact, there is no enhancement at 300 cm. Since the fraction of beam ions was also determined to fall off with distance (95% at 75 cm, 53% at 160 cm, and 32% at 300 cm), this observed enhancement could be linked to the effects of the high-speed flow. This change in enhancement level is most likely not due to the change in the effective size of the reference cylinder (2.0, 1.1, and 0.7 Debye lengths) since decreasing the size would theoretically have the opposite effect, that is, to increase the collected current per unit area rather than to decrease it as observed here. In addition, even if there were any residual end effects despite the use of guard structures, we believe that the enhancement could not be attributed to those end effects, since the strongest end effects should occur where the cylinder is the shortest in terms of the local Debye length (at 300 cm), whereas the observed enhancement is strongest where the cylinder length is the longest in terms of the Debye length (at 75 cm).

B. Solid Tapes

Fig. 7 also presents results for all solid tape samples at all three distances from the plasma source (75 cm, 160 cm, and 300 cm). The tape widths, shown in terms of the Debye length in the legend as well as in Table II, span from 4.9 to 41.9 electron Debye lengths. Three major observations are noted from these results.

1) All samples collect electrons less efficiently, on a per-area basis, than the reference cylinder, as is expected because of their larger size in terms of Debye lengths. Likewise, the collected current per unit area is seen to drop as the width of the tape is increased, regardless of its orientation. This is true whether we are looking at a mostly high-speed plasma (at 75 cm) or a mostly quiescent plasma (at 300 cm), and qualitatively agrees with the "current ratio" characteristic reported by Estes *et al.* [18, Fig. 4(b)] based on an equal-charge circular cylinder radius equal to one fourth of the tape width ($R_{eq} = 0.25 w_{\rm tape}$, [19]). Our collected current per unit area is somewhat lower than that predicted by Estes and Sanmartín [18], and is closer to, although still lower than, recent steady-state kinetic simulation results [16]. This remaining discrepancy in the current per unit area could be attributable to the presence of mounting screws that account for a small fraction of the total collecting area.

   These observations are in fairly good agreement with previous experimental data [7] that also showed a reduction in current per unit area as the effective tape width increased. Table VII shows a comparison of the collected current per unit area from data published by Gilchrist *et al.* [7] and the present data for parallel and perpendicular tapes (biased at an approximate normalized potential $\phi_0 \approx 100$), normalized with respect to the current per unit area collected on a thin cylinder. We find an excellent agreement for the furthest test position ($\sim$3-m range, $\sim 7\lambda_{\rm De}$ tape width), and a reasonable agreement at the closest test position

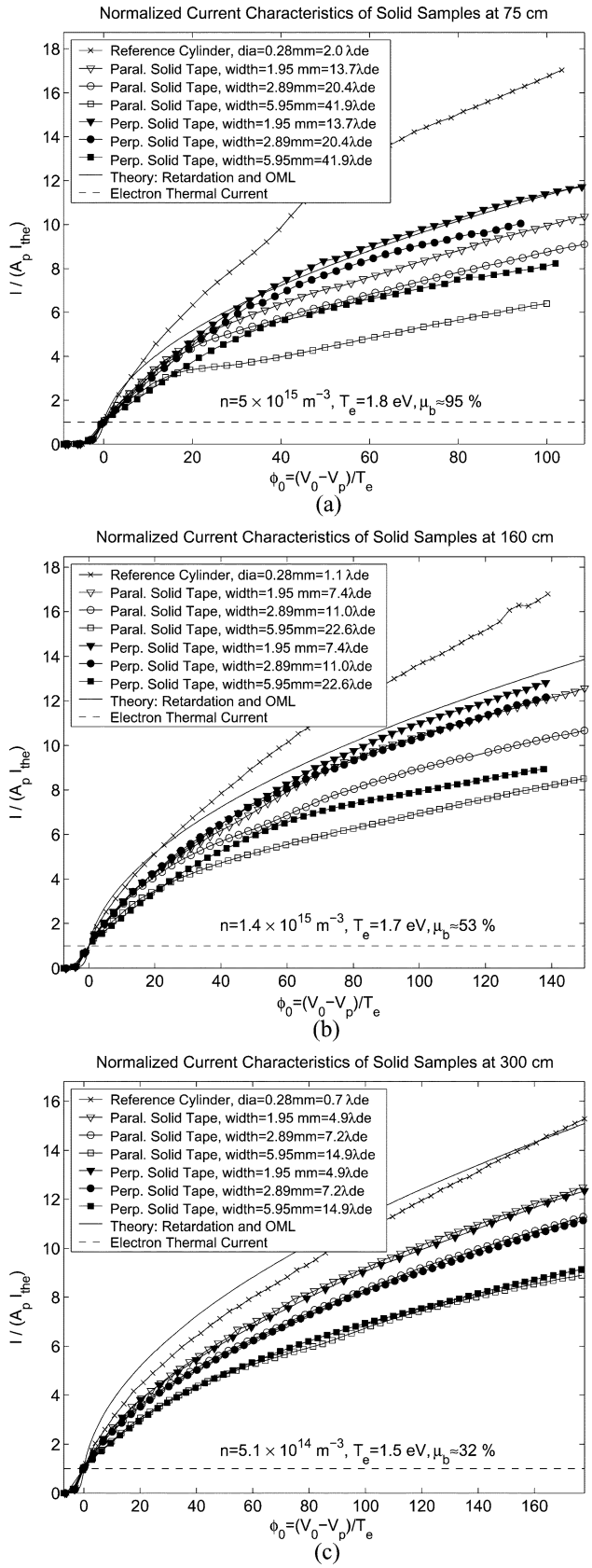

Fig. 7. Normalized *I–V* characteristics of parallel and perpendicular solid tapes at (a) 75 cm, (b) 160 cm, and (c) 300 cm.

($\sim$1-m range, $\sim 19-20\lambda_{\mathrm{De}}$ tape width). Note that the flow conditions were different in both data sets, which could explain the larger discrepancy at the closest distance where the high-speed fraction of the beam was found to be the highest.

2) At both the 75- and 160-cm distances, all solid tape samples collected more current when oriented perpendicular (transverse) rather than parallel to the flow. In addition, the contrast between perpendicular and parallel results is observed to get stronger as the width of the tape increases. However, such a clear distinction is not evident in the measurements taken at 300 cm, which is likely a consequence of the low fraction of beam ions that was measured at that location, combined with the smaller effective widths of the tapes (larger Debye length at that location) as compared to the two other locations. The near overlapping of the perpendicular and parallel results at 300 cm also serves as qualitative confirmation that the measured fraction of beam ions has dropped down as compared to that measured at 75 cm.

3) The previous observation of the increase of collected current when the tape probes are oriented transverse (perpendicular) to the flow is seen to occur when the probes are biased above a certain threshold, which varies from about 30 to 50 V. This level is on the order of the estimated ion beam energy (somewhere between 25 eV, according to the LP results, and 43 eV, according to the LIF results). At this threshold bias, the parallel results are seen to present a "knee," which is most apparent in the widest effective tape width at 75 cm. Previous results [7] have shown a similar knee occurring at a bias potential value close to the estimated flow energy.

TABLE VII
COMPARISON OF THE NORMALIZED COLLECTED CURRENT DATA (PER UNIT AREA) OBTAINED AT A NORMALIZED BIAS POTENTIAL $\phi_0 \approx 100$ BY GILCHRIST *et al.* [7] AND IN THE PRESENT PAPER. THE VALUES ARE NORMALIZED WITH RESPECT TO THE CURRENT PER UNIT AREA COLLECTED BY A THIN CYLINDER

Data Set	Tape Width	Normalized Collected Current Per Unit Area: Parallel Orientation	Normalized Collected Current Per Unit Area: Perpendicular Orientation
Gilchrist et al. [7], 305 cm	$6.9\lambda_{\mathrm{De}}$	85%	90%
Present Data, 300 cm	$7.2\lambda_{\mathrm{De}}$	85%	86%
Gilchrist et al. [7], 100 cm	$18.8\lambda_{\mathrm{De}}$	69%	77%
Present Data, 75 cm	$20.4\lambda_{\mathrm{De}}$	52%	62%

C. Slotted Tapes

Fig. 8 presents results for all slotted tape samples, as well as repeating the reference cylinder data at all three distances from the plasma source. The center-to-center line spacings, shown in terms of the Debye lengths in the legend, as well as in Table III, span from 1.4 to 13.2 Debye lengths. It should be emphasized that the overall widths of the slotted tapes, including the gap spacings, are the same as the solid tape widths (1.95 mm, 2.89 mm, and 5.95 mm) and the individual lines have the same perimeter as the reference cylinder. The following are some observations regarding these results.

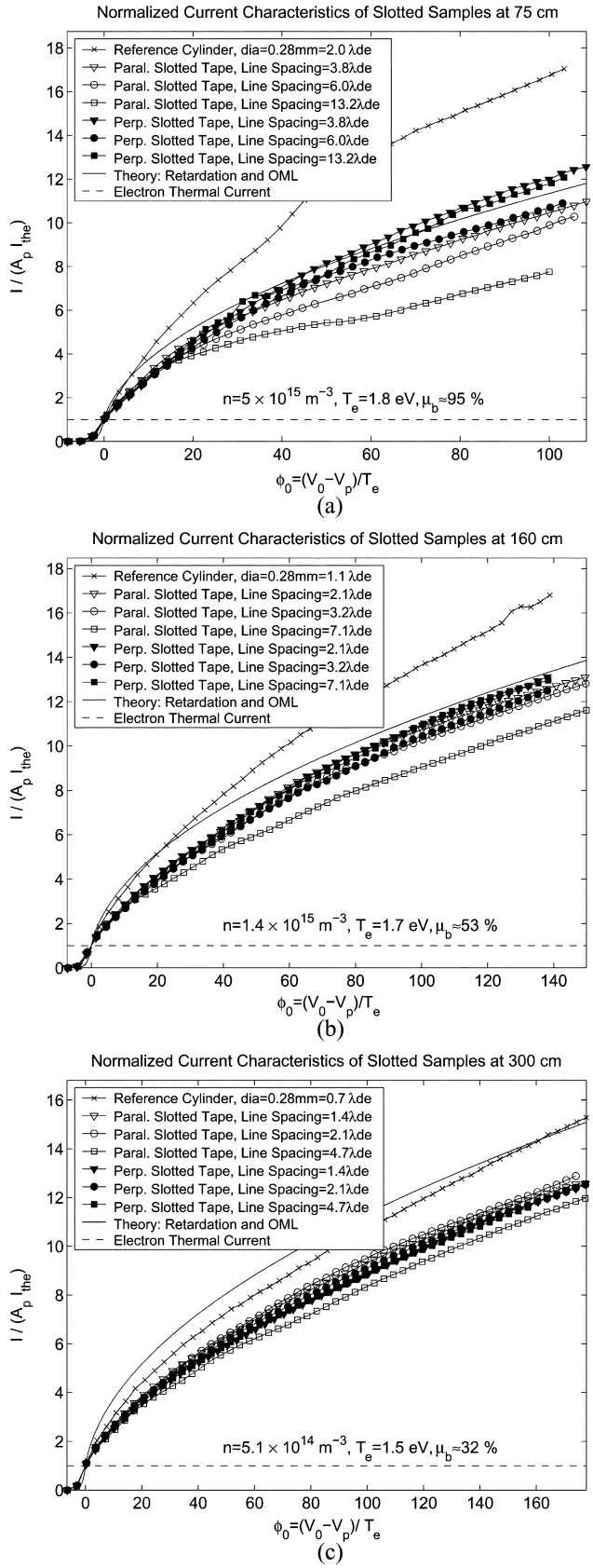

Fig. 8. Normalized *I–V* characteristics of parallel and perpendicular slotted tapes at (a) 75 cm, (b) 160 cm, and (c) 300 cm.

1) Similar to the tape results, the current per unit area collected by the slotted samples was lower than that collected on the reference cylinder at all three distances, although the slotted samples were more efficient electron collectors than the solid tapes. This is an indication that the sheaths of individual lines were strongly interacting.

2) The contrast between the results in the parallel and perpendicular (transverse) orientations has a similar character as that observed for the solid tapes: the perpendicular slotted tapes collect more current than their parallel counterparts. However, distinct from the solid tape results is the smaller variation between the responses of the three perpendicular slotted tape widths (especially at 75 cm and 160 cm) as compared to the parallel slotted ones. Specifically, the current per unit area collected on the widest (and most porous) slotted tape, with a line spacing of 13.2 Debye lengths at 75 cm, is roughly on par with that collected on the medium slotted tape (6.0 Debye lengths at 75 cm), and even exceeds it at the highest bias potentials. This may indicate that the widest line spacing was close to a critical value, corresponding to the minimum collected current, and beyond which the collected current would start increasing again, up to the very wide spacing limit where all four lines become independent and collect as efficiently as the reference cylinder. We seem to have attained this limit only in the perpendicular orientation, which might be explained by the fact that the sheath elongations in the direction of the flow [14], [15] would cause the sheath interactions to be more significant when aligned with (i.e., parallel to) the flow, thereby moving the critical spacing to a higher value for the parallel case. Clearly, testing of even wider line spacings will be required to determine those critical values and relate them to the flow energy. Recent kinetic simulations on parallel cylinders [16] have shown the theoretical existence of such a critical spacing for current collection.

3) A "knee" is most apparent in the results for the widest parallel slotted tape at 75 and 160 cm, around 23 and 19 V, respectively (note that the positions of the knees on the graphs need to be scaled with their respective electron temperatures and have values of 13 and 11, respectively, on the graphs), which is close to the estimated ion beam energy. The parallel and perpendicular results separate at the potential bias corresponding to the location of this knee.

D. Comparison of the Solid and Slotted Tapes

Figs. 9–11 show the same sets of results shown earlier, but with the solid and slotted tapes plotted on common graphs to facilitate their comparison. The absolute amount of current collected by the solid tape samples was higher than that collected by the slotted tape samples in all cases, as expected, and is not shown here. The slotted samples were somewhat more efficient on a per-area basis than their solid counterparts. This is true at all positions, and does not seem to be a function of the fraction of beam ions present. Hence, the slotted samples are always more efficient on a per-area basis, regardless of whether in a sta-

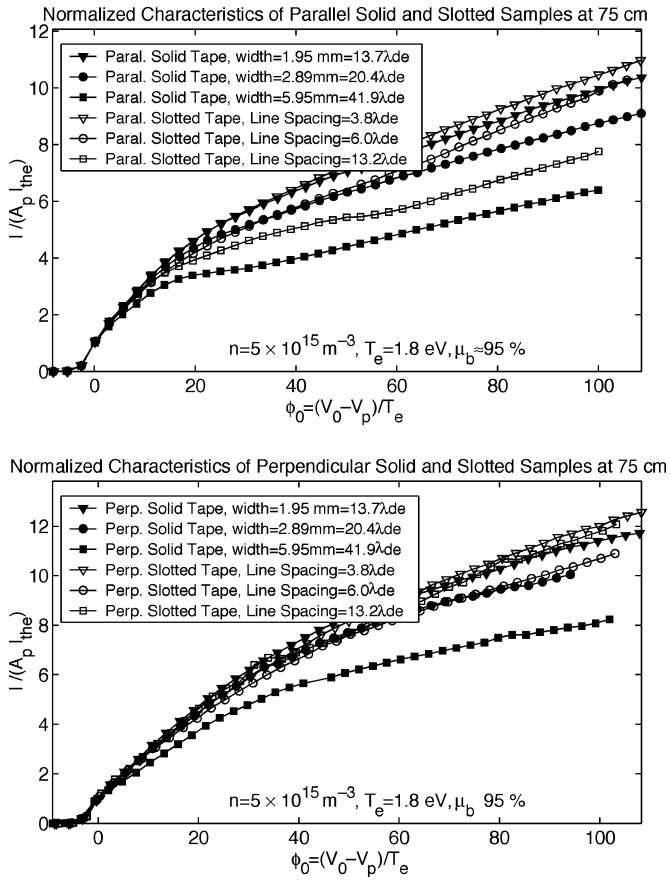

Fig. 9. Comparison of the *I–V* characteristics of solid and slotted tapes at 75 cm. Upper and lower graphs are applicable to parallel and perpendicular tape orientations, respectively.

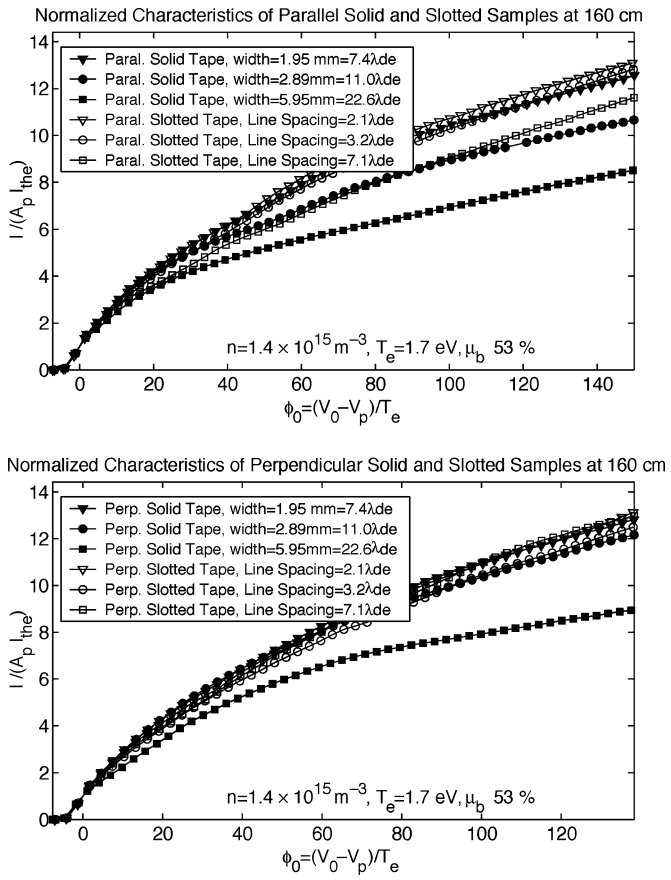

Fig. 10. Comparison of the *I–V* characteristics of solid and slotted tapes at 160 cm. Upper and lower graphs are applicable to parallel and perpendicular tape orientations, respectively.

tionary or flowing plasma. For example, at 75 cm, the parallel wide slotted tape collected about 37% of the current collected by the parallel wide solid tape at a normalized bias of 80 T_e, a somewhat higher fraction than the porosity of the sample, which was 28%.

VII. Present Status and Conclusion

Several conclusions can be drawn from the analysis of the results.

1) The plasma flow leads to significant enhancements of electron current collection over that predicted by the orbital-motion-limited theory.
2) The electron current per unit area collected to solid tapes decreases as the width of the tape is increased, a result consistent with earlier experiments [7].
3) Beyond a threshold bias close to the beam energy, solid and slotted tapes both collect more current when oriented transverse (perpendicular) to the flow.
4) Slotted tapes are more efficient electron collectors than solid tapes in terms of collected electron current per unit area.
5) Our data suggests that the current per unit area collected on slotted tapes decreases with increasing line spacing until a possible minimum current per unit area is attained, beyond which it is expected to start increasing again. The minimum may have been attained in the case of the samples oriented transverse to the flow, but not in the case of the samples aligned with the flow, for which the critical spacing is likely higher due to an increased sheath interaction radius of each line caused by the elongation of the sheath in the direction of plasma flow. Recent kinetic simulations on parallel cylinders [16] have shown the theoretical existence of such a critical spacing.

Further experiments are needed to more completely quantify the observed effects. In addition, larger line spacings should be tested in both the parallel and perpendicular orientations to verify the existence of and quantify the critical spacing that corresponds to the minimum collected current per unit area.

Finally, a lower background pressure might help improve the survival of the ion beam out to 3 m, and could possibly be achieved with the use of additional cryopumps. For example, using 7 cryopumps instead of 4 in the chamber, we could expect a drop of the background pressure by a factor 4/7, and consequently an increase of the charge-exchange mean-free-path length by a factor 7/4. Since the value shown for the high-speed beam fraction ($\mu_b = 32\%$) at 300 cm in Table V is consistent with a mean free path of about 2.6 meters, this additional pumping capacity could be expected to increase the mean free path to $2.6\ \mathrm{m} \times 7/4 \approx 4.6\ \mathrm{m}$. This should, therefore, improve the beam survival at 300 cm from 32% to about 52% ($\exp(-3.0\ \mathrm{m}/4.6\ \mathrm{m}) = 0.52$).

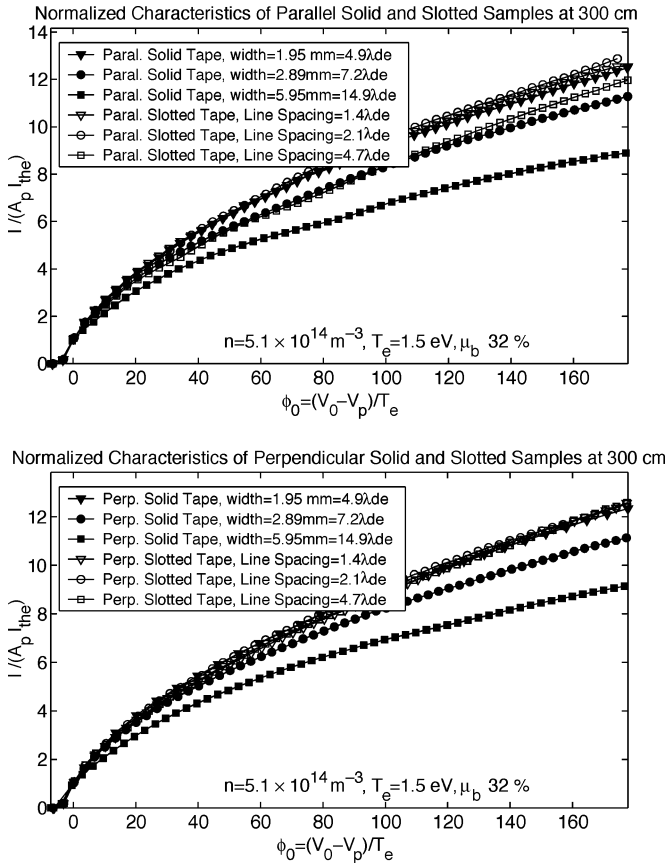

Fig. 11. Comparison of the *I–V* characteristics of solid and slotted tapes at 300 cm. Upper and lower graphs are applicable to parallel and perpendicular tape orientations, respectively.

APPENDIX
LANGMUIR PROBE ANALYSIS FOR DENSITY, TEMPERATURE, AND FLOW SPEED ASSESSMENT

The extraction of plasma parameters is an iterative procedure that requires several iterations of the "ion saturation analysis" and "electron retardation analysis," described below, to reach convergence. At every step, the electron retardation analysis is performed on the electron current exclusively, by removing the ion saturation best fit from the current data. Conversely, the ion saturation analysis is performed on the ion current alone by removing the latest best fit to the electron retardation region from the measured current.

A. Ion Saturation Analysis: Density $n_e \approx n_i$, Flow Energy $U_{\rm ev}$, and High-Speed Fraction μ_b

The OML ion current to a cylindrical probe biased negatively, $V_0 - V_p < 0$, in a plasma flowing at a velocity U and a corresponding "flow energy" $U_{\rm ev} = (m_i U^2/2e)$ is given by [13]

$$I_i = \sqrt{2}\frac{A_p e^{1.5}}{\pi\sqrt{m_i}} n_i \sqrt{\alpha T_i + U_{\rm ev} + V_p - V_0} \qquad (4)$$

where α is a constant between 1/2 and 1 depending on the flow energy. The slope of the linear fit to the I_i^2 versus V_0 LP data can be used to determine the plasma density $n_e \approx n_i$ (quasi-neutrality is strongly enforced within the plasma beam), while

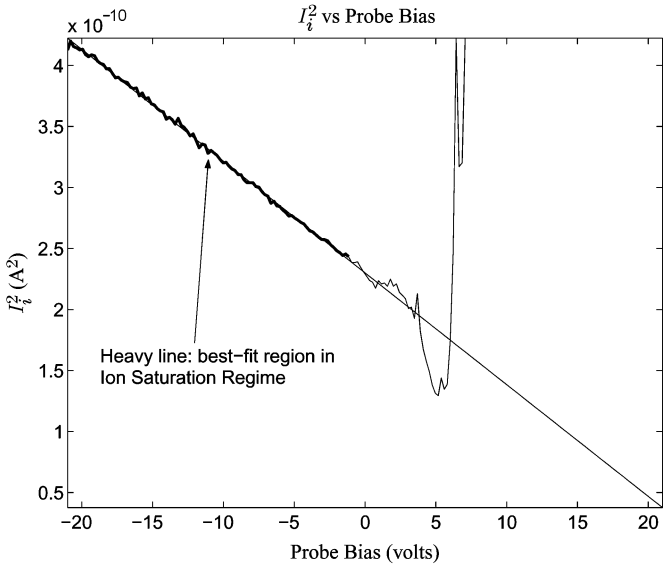

Fig. 12. Linear fit of the I_i^2 versus V data in the ion saturation regime, which is used to determine density, flow energy, and the fraction of beam ions.

the offset allows one to determine an estimate for the quantity $\alpha T_i + U_{\rm ev}$. An example of this procedure is shown in Fig. 12.

An additional feature was added to the analysis in order to account for the presence of a background of low-energy ions that have only thermal energy (i.e., they are not flowing), in addition to the beam of directed ions. If we suppose that a fraction μ_b of the ions are beam ions and that the low-energy ions have a temperature $T_{\rm slow}$, then the total ion current collected is given by

$$I_i = \sqrt{2}\frac{A_p e^{1.5}}{\pi\sqrt{m_i}} n_i \left\{ \mu_b \sqrt{\alpha T_i + U_{\rm ev} + V_p - V_0} + (1-\mu_b)\sqrt{T_{\rm slow} + V_p - V_0} \right\}. \qquad (5)$$

Neglecting the terms αT_i and $T_{\rm slow}$ which are both small with respect to the other terms, a best-fit procedure based on (5) was applied to the 75-cm LP data, assuming a high-speed fraction μ_b of 95% at this position. This yielded a beam energy of $U_{\rm ev} = 25$ eV, which is almost within the bounds of the error in the LIF result (43 eV $\pm$ 16 eV), as discussed in Section IV. Then, assuming that the flow energy of the high-speed population is constant at $U_{\rm ev} = 25$ eV across the three positions, fitting the 160-cm and 300-cm LP data into (5) yielded high-speed fractions of 53% and 32%, respectively. High-speed fractions obtained using this procedure for all three positions are summarized in Table V. We note that the error in the assumption of a 95% high-speed fraction at 75 cm, which we estimate is less than $\pm$5%, induces an error in the calculated beam energy $U_{\rm ev} = 25$ eV of less than 2 eV. However, density estimates are virtually unaffected (less than $\pm$0.2% effect) by this error in μ_b.

Evaluation of the Error in Density Estimates: Typically, the error in Langmuir probe density measurements is estimated based on the discrepancy between the electron and ion densities.

However, in the case of a flowing plasma, electron current collection is significantly enhanced, as is shown by our results, a phenomenon that no existing model can quantitatively predict. On the other hand, the effect of flow on ion current collection is very well understood, which means that plasma flow does not cause significant errors in the ion density estimates. Thus, the quantity $|n_e - n_i|$ would merely provide a measure of the error in the electron density introduced by the plasma flow.

Given that plasma flow does not contribute a significant error to the density estimate, we believe that the primary source of error in the determination of plasma density is the error in the Langmuir probe area estimate. We estimate the error in the length of the 4-cm Langmuir probe to be about ± 1 mm. As for the Langmuir probe's diameter of 0.28-mm, it is much more accurate due to precision manufacturing; it is estimated to have a 0.01-mm tolerance (actual tolerance could not be obtained from the manufacturer). Based on these two errors, the relative error in the probe area can be computed as $1/40 + 0.01/0.28 \approx \pm 6\%$.

Now, the collected ion current is proportional to the product of the probe area and plasma density. Thus, the $\pm 6\%$ relative error in probe area contributes a $\pm 6\%$ relative error in our density estimates. Secondary sources of error, such as secondary electron emission, the assumption discussed above regarding the high-speed fraction at 75 cm, as well as voltage and current measurement errors, should amount to less than $\pm 2\%$. In particular, the secondary electron emission yield for 100-eV xenon ions onto a tungsten target was measured to be about 1.3% [20]. Thus, we can safely argue that 20-eV ions would have a yield lower than 1% and, therefore, contribute less than $\pm 1\%$ of the error in plasma density. A conservative total error estimate would thus be obtained by the sum of $\pm 6\%$ (probe area) and $\pm 2\%$ (other errors), for a total of $\pm 8\%$.

Hall thrusters are known to produce a nonnegligible fraction of doubly charged ions at their nominal settings. However, due to the rather low discharge voltage used here ($V_d = 100$ V, see Table IV), only a small fraction of doubly-charged ions is expected. For the Hall thruster that was used in our tests, Gulczinski [21, Table 6.4] reports 6.8% of doubly-charged ions with a discharge voltage of 300 volts, and 16.4% at 500 volts. Although no data is available for a discharge voltage of 100 volts, we certainly do not expect more than a few percent of doubly charged ions. Nonetheless, their presence may lead to a slight overestimate of the actual ion density. However, our density estimates would still be consistent with the actual electron plasma density, assuming a quasineutral plasma beam. Since the electron density is really what we need for the analysis of our electron-collecting probe characteristics, we need not consider the existence of doubly charged ions as a significant error source.

B. Electron Retardation Analysis: Plasma Potential V_p and Electron Temperature T_e

Variations in the effective workfunction on the surface of our Langmuir probe (referred to as workfunction *patchiness* by Brace [22]) has turned out to be an area of concern in our experimental data. Our results appear to suggest a total effective workfunction variation of several electronvolts. Fig. 13 illustrates that effect, which leads to a departure from exponential behavior before the plasma potential is attained. Possible explanations for this variation could include polycrystalline workfunction variations of the tungsten probes (on the order of 1 eV, the tungsten workfunction being on the order of 4.5 eV), and possible surface contaminants, such as adsorbed residual gases and adsorbed xenon ions. A quantitative assessment of the contamination sources is outside of the scope of this paper, but we note here that several authors have linked effective workfunction variations to surface adsorbates [23]–[29].

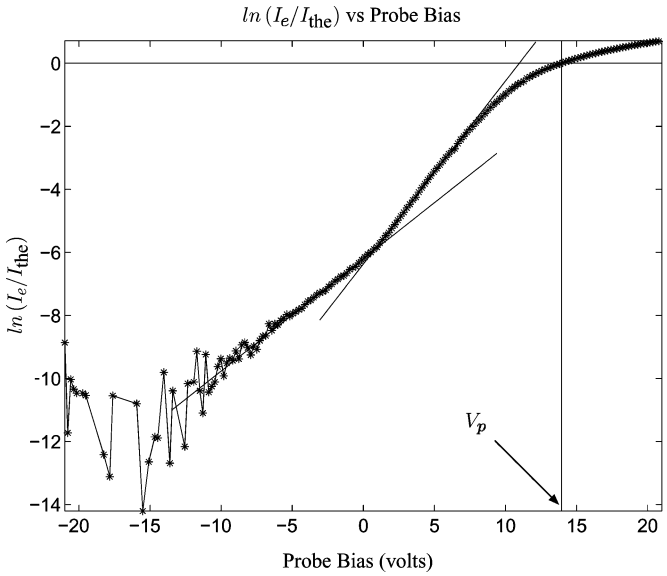

Fig. 13. Best fits in the electron retardation regime of a transverse-flow Langmuir probe. Two linear fits are performed on this semi-log plot. The one occurring at lower potential values corresponds to a population of warmer electrons, which account for just a few percent of the electron population.

A simple numerical experiment on the theoretical current collection characteristics of thin cylinders was performed in order to emulate the "blurring" effect of the workfunction variation. The results confirmed that the collected current at plasma potential stays within 3% of $I_{\rm the}$ as long as the workfunction variation is under 6.7 times the thermal temperature [16].

We use this feature of the OML blurring in our determination of the plasma potential. In other words, we locate the plasma potential by finding the potential where the collected current is equal to the electron thermal current. The cross-hair in Fig. 13 illustrates that result. As for the electron temperature, we may safely determine it based on the inverse of the slope of the retardation region at sufficiently low voltages, that is, beyond the reach of the blurring effect of the workfunction variation, as the rightmost linear fit shows in Fig. 13. Note that this procedure is performed on the electron current only, after the ion current has been removed from the total current data based on the best fit obtained within the ion saturation region. The leftmost linear fit shown in the same figure is identified with a population of warmer electrons, which account for just a few percent of the total electron population.

The temperature determination from the exponential fit of the retardation data is independent of the probe area, and as a consequence, the error in the Langmuir probe area estimate has

no bearing on the accuracy of the temperature estimate. The primary sources of error in the temperature determination are thus 1) the relative accuracy of the voltages measured by the Keithley 2410 sourcemeter that was used for the LP measurements, which is better than 1%; and 2) the empirical process used to select the voltage range over which a best fit of the retardation regime is performed. In order to be conservative in accounting for both of these error terms, we assume an overall accuracy of 5% for our temperature estimates.

Because the Debye length estimate is determined based on the estimated density and temperature values through the relationship $\lambda_{\mathrm{De}} = \sqrt{(\epsilon_0 T_e / e n_0)}$, the relative accuracy for Debye length, consistent with the 5% and 8% relative accuracy estimates for temperature and density, is obtained from

$$\frac{\Delta\lambda_{\mathrm{De}}}{\lambda_{\mathrm{De}}} = \frac{1}{2}\left(\frac{\Delta T_e}{T_e} + \frac{\Delta n}{n}\right) \approx \frac{1}{2}(5\% + 8\%) = 6.5\%. \quad (6)$$

ACKNOWLEDGMENT

The authors would like to thank T. Smith and D. Herman for support in performing those tests in the Large Vacuum Test Facility of PEPL.

REFERENCES

[1] J. Sanmartín, M. Martínez-Sánchez, and E. Ahedo, "Bare wire anodes for electrodynamic tethers," *J. Propulsion Power*, vol. 9, no. 3, pp. 353–360, 1993.

[2] H. Mott-Smith and I. Langmuir, "The theory of collectors in gaseous discharges," *Phys. Rev.*, vol. 28, pp. 727–763, 1926.

[3] L. Johnson, B. E. Gilchrist, R. D. Estes, E. Lorenzini, and J. Ballance, *Propulsive Small Expendable Deployer System (ProSEDS) Space Experiment*, 1998, AIAA Paper AIAA-98-4035.

[4] J. A. Vaughn, L. Curtis, B. E. Gilchrist, S. G. Bilén, and E. C. Lorenzini, *Review of the ProSEDS Electrodynamic Tether Mission Development*, Jul. 2004, AIAA Paper AIAA-2004-3501.

[5] J. V. Noord and R. Strumfels, *Electrodynamic Tether Optimization for the STEP-AirSEDS Mission*, 2001, AIAA Paper AIAA-2001-3980.

[6] J. Laframboise and L. Parker, "Probe design for orbit-limited current collection," *Phys. Fluids*, vol. 16, no. 5, pp. 629–636, May 1973.

[7] B. E. Gilchrist, S. G. Bilén, É. Choinière, A. D. Gallimore, and T. B. Smith, "Analysis of chamber simulations of long collecting probes in high-speed dense plasmas," *IEEE Trans. Plasma Sci.*, vol. 30, no. 5, pp. 2023–2034, Oct. 2002.

[8] J. M. Haas, F. S. Gulczinski II, A. D. Gallimore, G. G. Spanjers, and R. A. Spores, *Performance Characteristics of a 5 kW Laboratory Hall Thruster*, 1998, AIAA Paper AIAA-98-3503.

[9] B. E. Gilchrist, S. G. Bilén, É. Choinière, and A. D. Gallimore, "Laboratory experiments of current collection to long tape probes using a high-speed plasma relevant to bare electrodynamic tethers: Calibration and initial solid and slotted tape measurements," Univ. Michigan, Ann Arbor, Tech. Rep., 2002.

[10] G. J. Williams, Jr., T. B. Smith, M. T. Domonkos, K. J. Shand, A. D. Gallimore, and R. P. Drake, *Laser Induced Fluorescence Measurement of Ion Velocities in the Plume of a Hall Effect Thruster*, 1999, AIAA Paper AIAA-99-2862.

[11] T. B. Smith, D. A. Herman, and A. D. Gallimore, *Laser-Induced Fluorescence Velocimetry of Xe II in the 30-cm NSTAR-Type Ion Engine Plume*, July 2004, AIAA Paper AIAA-2004-3963.

[12] P. M. Chung, L. Talbot, and K. J. Touryan, *Electric Probes in Stationary and Flowing Plasmas: Theory and Application*. New York: Springler-Verlag, 1975.

[13] W. Hoegy and L. Wharton, "Current to a moving cylindrical electrostatic probe," *J. Appl. Phys.*, vol. 44, no. 12, pp. 5365–5371, Dec. 1973.

[14] É. Choinière and B. E. Gilchrist, *Electron Collection to Arbitrarily Shaped Electrodynamic Tethers in Flowing Plasmas: A Kinetic Model—Validation for Circular Cross-Sections*, Jul. 2002, AIAA Paper AIAA-2002-4050.

[15] ——, *Modeling Long Probes in Flowing Plasmas Using KiPS-2D, a Novel Steady-State Vlasov Solver*, 2003, AIAA Paper AIAA-2003-5098.

[16] É. Choinière, "Theory and experimental evaluation of a consistent steady-state kinetic model for 2-D conductive structures in ionospheric plasmas with application to bare electrodynamic tethers in space," Ph.D. dissertation, Univ. Michigan, Ann Arbor, 2004.

[17] S. G. Bilén, M. T. Domonkos, and A. D. Gallimore, "Simulating ionospheric plasma with a hollow cathode in a large vacuum chamber," *J. Spacecraft Rockets*, vol. 38, no. 4, pp. 617–621, Aug. 2001.

[18] R. Estes and J. Sanmartín, "Cylindrical Langmuir probes beyond the orbital-motion-limited regime," *Phys. Plasmas*, vol. 7, no. 10, pp. 4320–4325, Oct. 2000.

[19] J. Sanmartín and R. Estes, "The orbital-motion-limited regime of cylindrical Langmuir probes," *Phys. Plasmas*, vol. 6, no. 1, pp. 395–405, 1999.

[20] P. Varga and H. Winter, "Determination of metastable fractions in noble-gas-ion beams," *Phy. Rev. A*, vol. 18, no. 6, pp. 2453–2458, Dec. 1978.

[21] F. S. Gulczinski, "Examination of the Structure and Evolution of Ion Energy Properties of a 5 kW Class Laboratory Hall Effect Thruster at Various Operational Conditions," Ph.D. dissertation, Univ. Michigan, Ann Arbor, MI, 1999.

[22] "Langmuir Probe Measurements in the Ionosphere," L. H. Brace, in *Measurement Techniques in Space Plasmas: Particles*. Washington, DC: Amer. Geophys. Union, 1998, pp. 23–35.

[23] G. Wehner and G. Medicus, "Reliability of probe measurements in hot cathode gas diodes," *J. Appl. Phys.*, vol. 23, no. 9, pp. 1035–1045, Sep. 1952.

[24] C. Winkler, D. Strele, S. Tscholl, and R. Schrittwieser, "On the contamination of Langmuir probe surfaces in a potassium plasma," *Plasmas Phys. Controlled Fusion*, vol. 42, pp. 217–223, 2000.

[25] B. Waclawski and L. Hughey, "Adsorption of water vapor on polychrystalline tungsten," *Surface Sci.*, vol. 19, pp. 464–468, 1970.

[26] M. J. Dresser, T. E. Madey, and J. T. Yates, Jr., "The adsorption of xenon by W(111), and its interaction with preadsorbed oxygen," *Surface Sci.*, vol. 42, pp. 533–551, 1974.

[27] H. Miki, H. Inomata, K. Kato, T. Kioka, and K. Kawasaki, "Chemisorption of NO on polychrystalline tungsten surface," *Surface Sci.*, vol. 141, pp. 473–486, 1984.

[28] T. Kioka, A. Kawana, H. Miki, S. Sugai, and K. Kawasaki, "Chemisorption of NO on W(100) and W(110) surfaces studied by AES and UPS," *Surface Sci.*, vol. 182, pp. 28–40, 1987.

[29] E. Stamate and K. Ohe, "Influence of surface condition in Langmuir probe measurements," *J. Vac. Sci. Technol.*, vol. 20, no. 3, pp. 661–666, 2002.

Éric Choinière (S'98–M'04) received the B.Eng. and M.S. degrees in electrical engineering from École Polytechnique de Montréal, Montréal, Canada in 1997 and 1999, respectively, and the Ph.D. degree from the University of Michigan, Ann Arbor, in 2004. The research work that led to his M.S. thesis involved the development of a computational model for multilayered printed array antennas and frequency selective surfaces. His Ph.D. work focused on the development of a new steady-state 2-D kinetic plasma model for conductive structures in flowing plasmas, in addition to related experimental investigations in vacuum environments.

He is currently a Defence Scientist with Defence Research and Development Canada, Ottawa, as well as a research associate with the Electrical Engineering and Computer Science Department, University of Michigan, Ann Arbor. His current research interests involve the computational modeling of space plasmas for bare space tether applications, as well as the design of multiband antennas for software-defined-radio satellite terminals.

Dr. Choinière is a Member of the American Geophysical Union.

Sven G. Bilén (S'90–M'98) received the B.S. degree from Pennsylvania State University, Philadelphia, in 1991 and the M.S.E. and Ph.D. degrees from the University of Michigan, Ann Arbor, in 1993 and 1998, respectively. His Ph.D. work examined the general propagation behavior of high-voltage EM pulses along conductors in low-density, cold plasmas with the specific application of electrodynamic tethers in the ionosphere

In January 2000, he joined Pennsylvania State University as an Assistant Professor in Electrical Engineering and in Engineering Design. He currently serves as the Chief Technologist for the Center for Space Research Programs at Pennsylvania State University. His related research interests include electrodynamic-tether science, technology, and applications, *in situ* measurements of space plasmas and environments, circuit modeling of plasmas and spacecraft-plasma interactions, and plasma diagnostics for space plasmas, plasma electric thrusters, and semiconductor plasma processing.

Dr. Bilén is a Member of the American Institute of Aeronautics and Astronautics, American Geophysical Union, American Society for Engineering Education, and Sigma Xi.

Brian E. Gilchrist (S'75–M'78–SM'03) received the B.S. and M.S. degrees from the University of Illinois, Urbana, in 1977 and 1979, respectively, and the Ph.D. degree from Stanford University, Stanford, CA, in 1991, all in electrical engineering.

He is currently Professor of electrical engineering, space science, and applied physics at the University of Michigan, Ann Arbor. He is also Associate Chair for the Electrical and Computer Engineering Division of the Electrical Engineering and Computer Science Department. He acquired 12 years of industrial microwave systems and technology research and development experience prior to receiving the Ph.D. degree. His primary research interests include developing electrodynamic tethers as a new propellantless space propulsion technology, ion and electron emitter technology, plasma diagnostics for the ionosphere and for plasma electric propulsion systems, and spacecraft technology. He is a member of the Radiation and Space Physics Research Laboratories at Michigan.

Dr. Gilchrist is an Associate Fellow of the American Institute of Aeronautics and Astronautics and a Member of the American Geophysical Union and American Society for Engineering Education.

Keith R. Fuhrhop (S'98) received the B.S. degree in engineering physics from Syracuse University, Syracuse, NY, in 2000, and the M.S. degree in electrical engineering from the University of Michigan, Ann Arbor, MI, in 2002. He is currently working toward the Ph.D. degree in electrical engineering at the University of Michigan, Ann Arbor, and is affiliated with the Radiation Laboratory and the Space Electrodynamics and Tether Systems Group. His M.S. research involved designing an experiment to test the ion cyclotron resonance heating for use in electromagnetic propulsion, as well as magnetometer analysis for use in the University of Michigan's ICARUS student-fabricated satellite.

His current research involves the analysis of bare electrodynamic space tethers and current collection processes of orbiting bodies in the Earth's ionosphere.

Mr. Fuhrhop is a Member of the American Institute of Aeronautics and Astronautics and the American Nuclear Society.

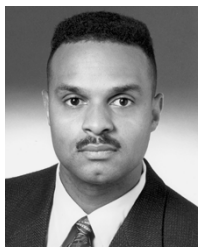

Alec D. Gallimore received the B.S. degree in aeronautical engineering from Rensselaer Polytechnic Institute, Troy, NY, in 1986, and the M.A. and Ph.D. degrees in aerospace engineering from Princeton University, Princeton, NJ, in 1988 and 1992, respectively.

He is currently a Professor of Aerospace Engineering and Applied Physics at the University of Michigan, Ann Arbor, where he directs the Plasmadynamics and Electric Propulsion Laboratory. His primary research interests include electric propulsion, plasma diagnostics, space plasma simulation, and electrode physics. He has experience with a wide array of electric propulsion technologies, including MPD thrusters, arcjets, ion engines, and Hall thrusters, and he has implemented a variety of probe, microwave, and optical plasma diagnostics.